Ann. For. Res. 65(1): 9935-9946, 2022
ISSN: 18448135, 20652445

ANNALS OF FOREST RESEARCH
https://www.e-afr.org/

A HISTOLOGICAL MICROSCOPIC VIEW OF THE WHITE MOUSE BRAIN DOSED EXPERIMENTALLY WITH *ESCHERICHIA COLI* O157:H7 AND TREATED WITH A DRUG AND ANTIBIOTIC

Ateen Amer Hameed, Prof. Dr. Khulood Naji Rasheed, Prof. Dr. Hala Mohammed Majeed

Abstract

The research is conducted to detect the pathogenicity of *E. coli* O157: H7 and know the effects of its experimental infection in the histological structure of the brain of male mice at the age of (8-12) weeks, In addition, it attempts to determine the therapeutic effect of an approved drug in the treatment of bacteria and compare it with an antibiotic whose effectiveness is tested *in vitro*. The antibiotic sensitivity test results show that the bacteria are sensitive to Trimethoprim-Sulfamethoxazole, Metronidazole, Gentamicin, Amikacin, Tetracycline, Azithromycin, Ceftriaxone and Ciprofloxacin, and resistant to Amoxicillin/clavulanic acid and Ampicillin. The most sensitive antibiotic is Ciprofloxacin, followed by Trimethoprim-Sulfamethoxazole. As the latter is an approved and widely used antibiotic, it is chosen with Ciprofloxacin to determine their therapeutic effect against the bacteria under study. Animals experimentally infected with this bacteria show different degrees of clinical signs represented by lethargy, recluse, loss of appetite, increase in respiratory rate and heart beat rate with different degrees of diarrhea appearing in a number of them. In others different forms of paralysis appear, either paralysis of the hind feet or complete immobility, in addition, to the occurrence of a number of deaths in mice infected experimentally with the infectious dose of bacteria. As for the results of the histological examination they are vaculation in the outer molecular layer, hyperplasia in the outer granular layer and part of it necrosis, loss of chromatin material for the nuclei of the cells of the polymorphic layer, detachment of the meningeal membranes, congestion of blood vessels as well as hemorrhage and inflammatory cellular infiltration and these symptoms are more severe in the half-lethal (LD-50) dose group. As for the groups treated with the two aforementioned antibiotics it is noted that they play an effective role in stopping diarrhea with mice somewhat regaining their activity, However they still had suffered from various tissue lesions represented by necrosis, vacuolation, degeneration, inflammatory cellular infiltration, congestion and hemorrhage.

1.Introduction

Escherichia coli belongs to the Enterobacteriaceae, and it is an endemic normal flora of the large intestine in humans and other mammals (Sejal and Leonard, 2015). This harmless bacterium usually becomes a highly adaptive pathogen, capable of causing various diseases in healthy individuals, especially those suffering from immunodeficiency by obtaining a mixture of mobile genetic elements (Li *et al*., 2019).

Enterohemorrhagic *Escherichia coli* is regarded as the leading cause of outbreaks of diarrheal diseases, hemolytic uremic syndrome (HUS), and hemorrhagic colitis (HC) in humans and animals (Tse *et al*., 2018). The O157:H7 serotype is a common pathogen between humans and

animals, transmitted through food and is responsible for most cases of enterohaemorrhagic diarrhea in humans (Dulo, 2014).

The mechanism followed by this bacteria in causing pathogenicity is not fully understood, but the virulence factors that it possesses have a major role in the occurrence of the disease, the most important of which is the Shiga toxins. The bacteria that produce Shiga toxin are called Shiga Toxin *E. coli* (STEC). It causes damage to the intestinal vascular lining, and this effect has been observed in people with hemorrhagic colitis and hemolytic uremic syndrome (Fatima and Aziz, 2019). It also has the ability to resist the acidic environment, produce the hemolysin enzyme, possesses fimbriae that adhere to the epithelial cells of the urinary system, as well as flagella that make it able to adhere to the cells lining the intestine. In addition, it leads to the formation of adhesion lesions and damage to the intestinal villi, which leads to a decrease in the absorption capacity of the intestinal mucosa and thus an imbalance in the ion balance leading to the occurrence of diarrhea (Feng *et al.*, 2014).

E.coli O157:H7 producing shiga toxin (Stx) causes neurological signs as well as bloody diarrhea and hemolytic uremic syndrome. as approximately 30% of people with HUS suffer from nervous system disorders (Obrig, 2010). Stx2 is widely associated with the appearance of neurological signs compared with Stx1. Moreover, the mechanism of access of the toxin to the brain is conducted by binding with the Globotriaosylceramide (Gb3) receptors present in the target cell, as it reaches the endoplasmic reticulum, inhibits protein synthesis and thus causes damage to the vascular endothelial cells of the system neurological disease leading to neurological signs (Legros *et al.,* 2018).

2. Materials and methods

2.1 Chemicals and culture agars

The traditional MacConkey agar is used to isolate the bacteria. SMAC agar is used to confirm its diagnosis, While HiCrome agar is regarded as one of the selective media for *E.coli* O157:H7 as EMB agar. The chemicals formalin, ethanol, xylene, paraffin, Hematoxylin, Eosin, and D.P.X are used in the preparation of histological sections of the brain.

2.2 Bacterium Isolate

The diagnosed and ready-to-use *E.coli* O157:H7 isolate is used. Despite this, some culture laboratory tests are performed to confirm the validity of its diagnosis. Its type is also determined by biochemical tests using the VITEK® 2 Compact device. The Antibiotic susceptibility testing is carried out using the modified Bauer-Kirby method (Bauer *et al.*, 1966) approved by the World Health Organization.

2.3 Determination of the half lethal dose (LD-50), the infectious dose and the bacterial count

The LD-50 dose and the infectious dose are determined according to the Reed - Muench method (1938). As for the bacterial count, the Pour plate method is used for its determination.

2.4 The Experimental Design

Forty-eight male mice of the Balb/c strain, aged (8-12) weeks, weighing between (22-28) gm, are used. They are randomly distributed into six groups of (8) mice per group as follows:

1- The first group (the control group): a group of mice treated with physiological solution at a rate of 1 ml once a day.
2- The second group: a group of mice treated with the LD-50 dose of *E.coli* O157:H7 at a concentration of 9×10^2 cell/ml.
3- The third group: a group of mice treated with the infectious dose of bacteria at a concentration of 5×10^5 cell/ml.
4- The fourth group: a group of mice treated with the antibiotic Trimethoprim-Sulfamethoxazole by 1 ml per day at a concentration of 102.88 mg / kg according to Nair and Jacob (2016).
5- The fifth group: a group of mice treated with the antibiotic Ciprofloxacin by 1 ml at a concentration of 102.88 mg / kg according to Nair and Jacob (2016).
6- The sixth group: a group of mice treated with the two antibiotics together, Trimethoprim-Sulfamethoxazole and Ciprofloxacin, at a concentration of 102.88 mg/kg each.

Glass slides of brain tissue are then made via the sectioning method using the Luna (1968) method, which includes: fixation, washing, dehydration, clearing, infiltration , embedding, trimming and sectioning, staining, and mounting. Finally, the tissue glass slides are examined are then examined and photographed under a light microscope at different magnification powers.

3. Results and Discussion

3.1 Confirming the diagnosis of *E.coli* O157:H7

The diagnosis of the bacteria under study and its type is confirmed based on the bacterial isolation via traditional and selective culture agars and biochemical tests using the Vitek device as illustrated in Figures (3-1), (3-2), (3-3), (3-3), (3.4) and Table (3-1).

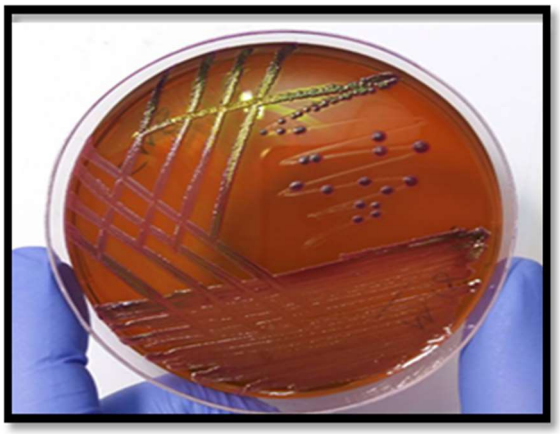

Figure (3-1) *E.coli* on EMB agar

Figure (3-2): *E.coli* on solid MacConkey agar

Figure (3-3): *E.coli* O157:H on SMAC agar

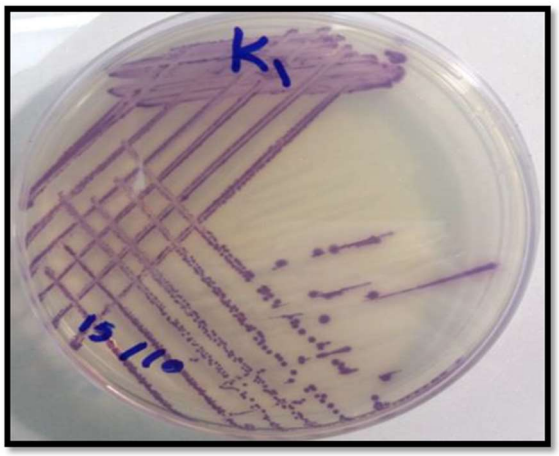

Figure (3-4): *E.coli* O157:H7 on HiCrome agar

Table (3-1): Biochemical diagnosis using the Vitek device

Identification Information	**Card:** GN	**Lot Number:** 2411419403	**Expires:** Oct 15, 2021 13:00 CDT
	Status: Final	**Analysis Time:** 10.00 hours	**Completed:** Apr 2, 2021 12:23 CDT
Organism Origin	VITEK 2		
Selected Organism	98% Probability **Escherichia coli O157** Bionumber: 0405611140567251 Confidence: Excellent identification		
Analysis Organisms and Tests to Separate:			
Analysis Messages: Confirm by serological tests Highly pathogenic organism			
Contraindicating Typical Biopattern(s) Escherichia coli O157 SAC(80),			

Biochemical Details																	
2	APPA	-	3	ADO	-	4	PyrA	-	5	lARL	-	7	dCEL	-	9	BGAL	+
10	H2S	-	11	BNAG	-	12	AGLTp	-	13	dGLU	+	14	GGT	-	15	OFF	+
17	BGLU	-	18	dMAL	+	19	dMAN	+	20	dMNE	+	21	BXYL	-	22	BAlap	-
23	ProA	+	26	LIP	-	27	PLE	-	29	TyrA	+	31	URE	-	32	dSOR	-
33	SAC	-	34	dTAG	-	35	dTRE	+	36	CIT	-	37	MNT	-	39	5KG	-
40	lLATk	+	41	AGLU	-	42	SUCT	+	43	NAGA	-	44	AGAL	+	45	PHOS	+
46	GlyA	+	47	ODC	+	48	LDC	+	53	lHISa	-	56	CMT	+	57	BGUR	-
58	O129R	+	59	GGAA	-	61	lMLTa	+	62	ELLM	+	64	lLATa	-			

Our results agree with Al-Taie (2020) in his study of isolating and diagnosing *E.coli* O157:H7. They appear as pink colonies on the MacConkey agar since they ferment lactose sugar, while characterized by the phenomenon of metallic luster on EMB agar. Our results also agree with Yadav *et.al* (2018) in the appearance of typical colonies of these colorless bacteria as they do not ferment the sorbitol sugar on SMAC agar, while the pink-purple colonies indicate *E.coli* O157:H7. In a study performed by Klaif *et. al* (2019), they found that HiCrome agar of *Escherichia coli* bacteria of the O157:H7 serotype is useful for the diagnosis of this bacteria.

3.2 Testing the sensitivity of *E.coli* O157:H7 to antibiotics

A sensitivity test is conducted towards (10) types of different antibiotics. The results show that the bacteria are sensitive to the antibiotics Trimethoprim-Sulfamethoxazole, Metronidazole, Gentamicin Amikacin, Azithromycin, Ceftriaxone, Ciprofloxacin and Tetracycline, and resistant to Amoxicillin/clavulanic acid and Ampicillin. It is noted that the bacteria are more sensitive to the antibiotic Ciprofloxacin, followed by the antibiotic Trimethoprim-Sulfamethoxazole, as shown in Figures (3-5) and (3-6).

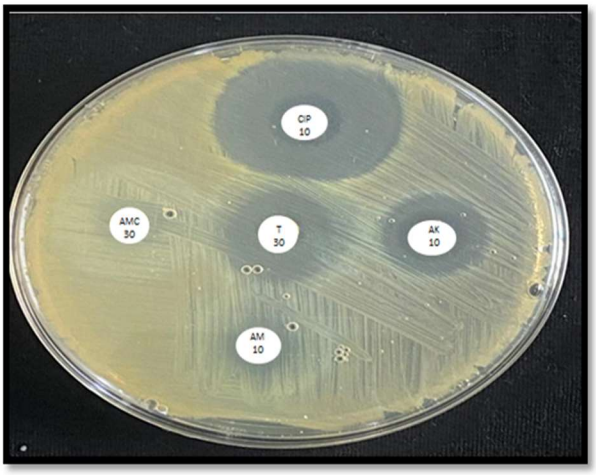

Figure (3-5): Bacteria sensitivity to Amikacin, Tetracycline and Ciprofloxacin and their resistance to Amoxicillin/clavulanic acid and Ampicillin

Figure (3-6): Bacteria sensitivity to the antibiotics Trimethoprim-Sulfamethoxazole,Metronidazole, Gentamicin, Azithromycin and Ceftriaxone

The current results agree with the results of Tawfiq (2006) in his study on coliform bacteria isolated in hospitals in the Kingdom of Saudi Arabia, with their resistance to ampicillin being high. In addition, it confirms the results of Ali (2012) which supported these results, with the exception of his results in the resistance of the bacteria to the antibiotics Trimethoprim and Amoxicillin/ clavulanic acid. Here, our results do not agree with his, nor do they agree with Nguyen *et al*. (2005) who reached the same conclusions. As for our results regarding the sensitivity of *E.coli* to Ciprofloxacin and Trimethoprim, they agree with the results of Mahdi (2019).

3.3 The Histological Examination

The microscopic examination of the first group shows the normal appearance of the layers of the cerebral cortex consisting of the molecular/plexiform layer, the outer granular layer, the outer pyramidal layer, the inner granular layer, the inner pyramidal layer and the polymorphic cell layer, as well as the normal appearance of Cajal cells in the molecular layer and the normal appearance of capillaries as in figures (3-7), (3-8), (3-9). As for the second group, the histological changes are represented by the loss of chromatin in the nuclei of cells of the polymorphic layer, the occurrence of acute vacuolation throughout the molecular layer and their rupture in the areas of separation of the meninges from the cerebral cortex, the occurrence of vacuolar degeneration of the supporting glial cells, the emergence of acute congestion in the blood vessels of the arachnoid membrane with its rupture and the infiltration of inflammatory cells as shown in Figures (3-10), (3-11), (3-12). It is also observed that the outer molecular layer is erupted, hyperplasia of the outer granular layer and necrosis of part of it, its sharp reduction and confinement to separate cells in other sections, hypertrophy of its cells, slight hemorrhage in the pia mater membrane, its separation from the meningeal membranes, complete loss of the meningeal membrane, as well as the appearance of some blood vessels congested with blood in the mice of the third group, as shown

in Figures (3-13), (3-14), (3-15). As for the histological changes in the fourth group, they are limited to the appearance of blood congestion at the periphery of the pia mater meningeal membrane, vacuolar degeneration in the cells of the polymorphic layer, as well as the disintegration of some nerve fibers, as in Figures (3-16) and (3-17). There is some improvement in the brain tissue of the mice of the fifth group, with the exception of slight hemorrhage, thrombosis, as well as vacuolization of some nerve fibers, and an accumulation of supportive glial cells, as in Figures (3-18) and (3-19). As for the sixth group, the normal appearance of nerve cells and glial cells in shape and size is observed. There is the survival of few histological changes represented by blood congestion at the periphery of the pia mater membrane and in the molecular layer, with a slight disintegration of nerve fibers, as in Figures (3-20) and (3-21).

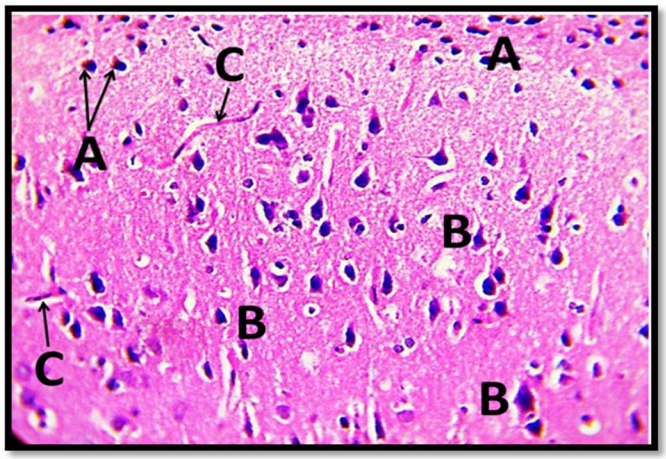

Figure (3-8): A microscopic image of a section in the brain of a mouse from the first group, in which the normal appearance of two layers of the cerebral cortex is noted, where the inner granular layer composed of stellate neurons in the form (A), and the inner pyramidal layer composed of The pyramidal-shaped neurons are the largest among the neurons in the layers of the cerebral cortex (B), as well as the normal appearance of the capillaries (C). (H&E, X40).

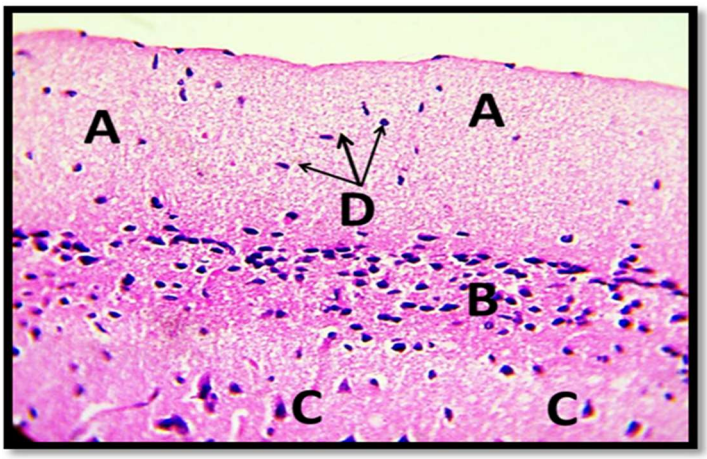

Figure (3-7): A microscopic image of a section in the brain of a mouse from the first group, in which the normal appearance of three layers of the cerebral cortex is noted, where the molecular or plexiform layer consisting of nerve fibers is located parallel to the surface (A), layer The outer granular layer of small pyramidal neurons (B), the outer pyramidal layer of medium-sized pyramidal neurons (C), as well as the normal appearance of Cajal's neurons (D) in the molecular layer. (H&E, X40).

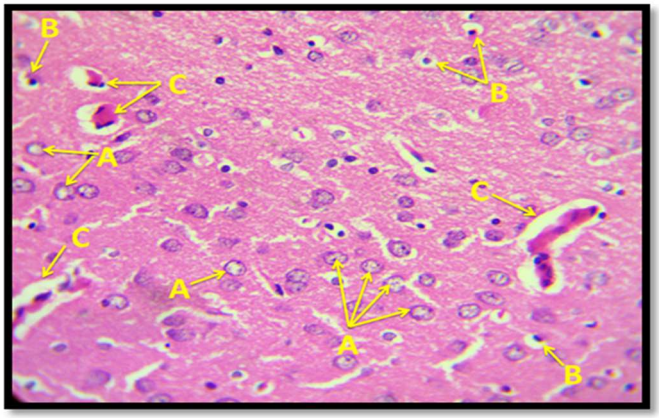

Figure (3-10): A microscopic image of a section in the brain of a mouse from the second group, in which a layer of polymorphic cells is observed where some of its nuclei have lost chromatin (A), vacuolar degeneration of the supporting glial cells (B), as well as a bloody congestion in some vessels (C). (H&E, X40).

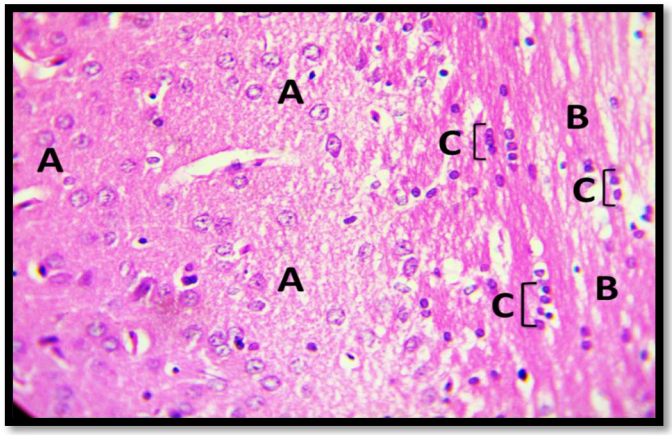

Figure (3-9): A microscopic image of a section in the brain of a mouse from the first group, in which the normal appearance of the polymorphic or multiform layer, which is the innermost among the layers of the cerebral cortex (A) and close to the white matter (B), is noted, as well On the appearance of normal neuroglial cells (C) between nerve fibres. (H&E, X40).

Figure (3-12): Microscopic image of a section in the brain of a mouse from the second group, in which dilatation and acute congestion of blood vessels (A) in the arachnoid membrane of the meninges (B), rupture of the arachnoid membrane (C), and infiltration of inflammatory cells (D) are noted.). (H&E, X40).

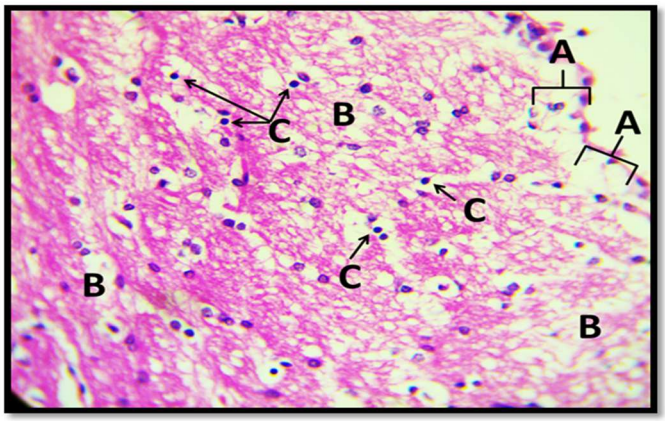

Figure (3-11): Microscopic image of a section in the brain of a mouse from the second group, in which the meninges separate from the cerebral cortex and rupture in the molecular layer at the separation area (A), severe vaculation throughout the molecular layer (B), cellular inflammatory infiltration cells infiltration (C). (H&E, X40).

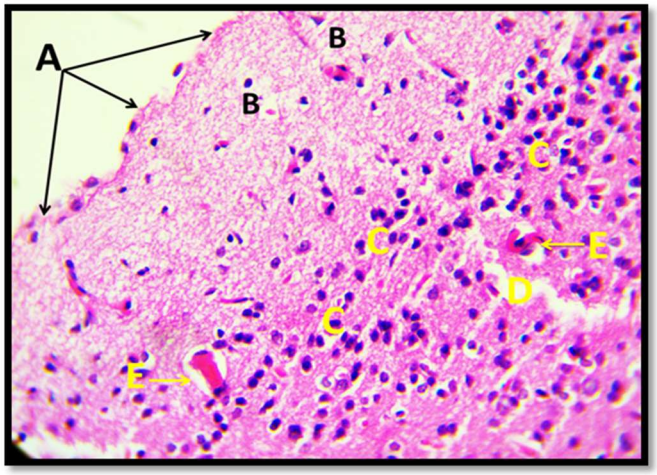

Figure (3-14): Microscopic image of a section in the brain of a mouse from the third group, in which the loss of the meninges (A), vacuolation of the molecular layer (B), hyperplasia of the outer granular layer (C) and necrosis in part of it (D) are noted. vascular congestion (E). (H&E, X40).

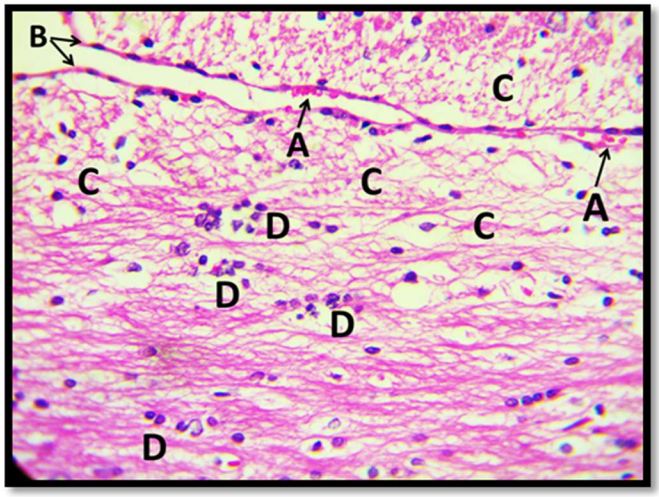

Figure (3-13): Micrograph of a section of the brain of a mouse from the third group, in which slight hemorrhage (A) is observed in the meningeal pia mater (B), vacuolation of the molecular layer (C), and a sharp reduction and confinement of the outer granular layer

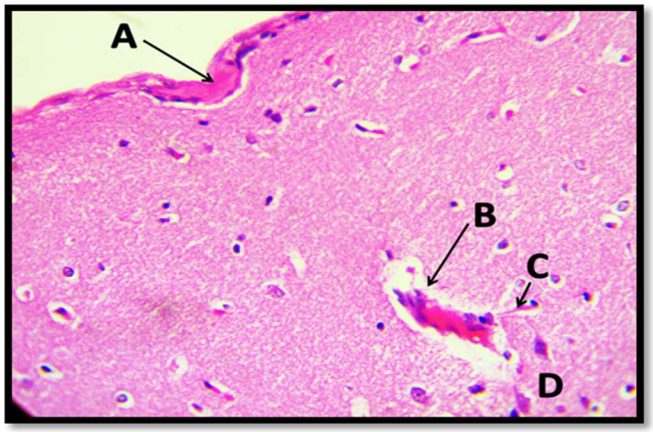

Figure (3-16): Microscopic image of a section of the brain of a mouse from the fourth group, in which blood congestion is observed (A) at the periphery of the pia mater meningeal (B) and between the outer granular layers (C) and the outer pyramidal layers (D). (H&E, X10).

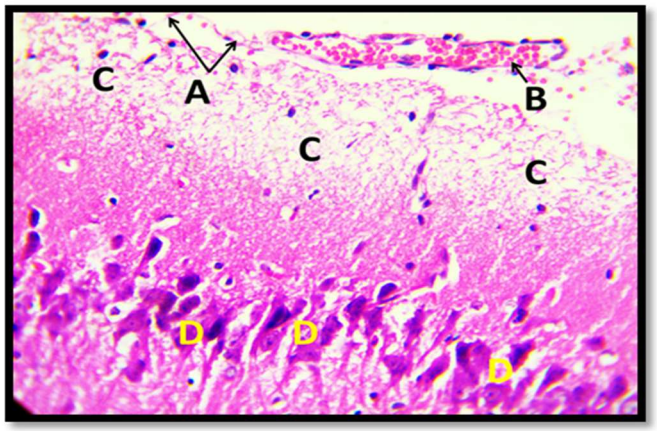

Figure (3-15): Microscopic image of a section in the brain of a mouse from the third group, in which detachment of the pia mater meningeal membrane (A), dilatation and congestion of a blood vessel (B), extensive vacuolation in the molecular layer (C), hypertrophy in the cells of the The outer granular layer (from small pyramidal to giant pyramidal cells) (D). (H&E, X40).

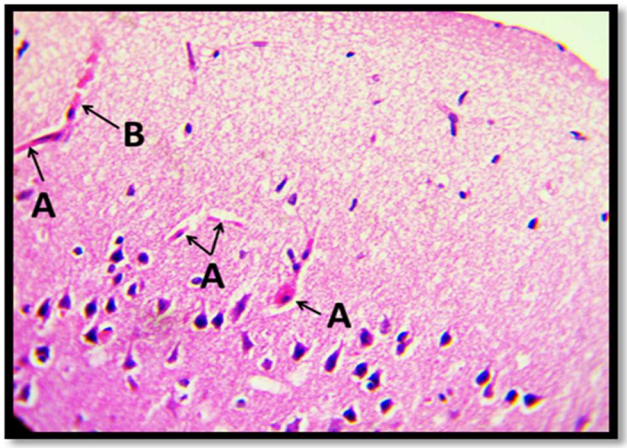

Figure (3-18): Microscopic image of a section of the brain of a mouse from the fifth group, in which capillaries congested with blood are observed (A), slight hemorrhage (B). (H&E, X40).

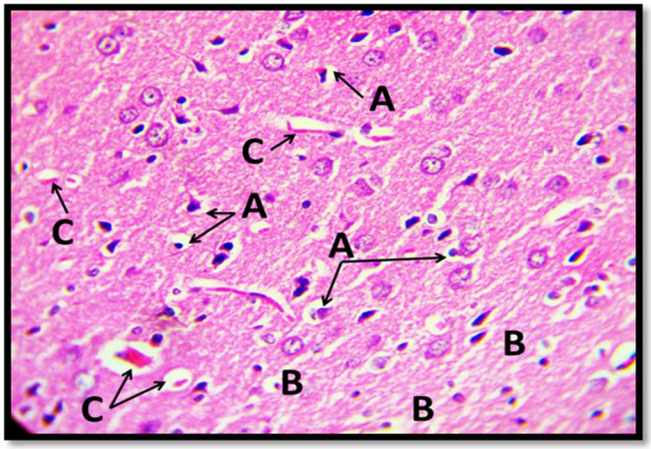

Figure (3-17): A microscopic image of a section in the brain of a mouse from the fourth group, in which vacuolar degeneration is observed in the cells of the polymorphic layer (A), in addition to the disintegration of nerve fibers (B), congestion in some capillaries (C). (H&E, X40).

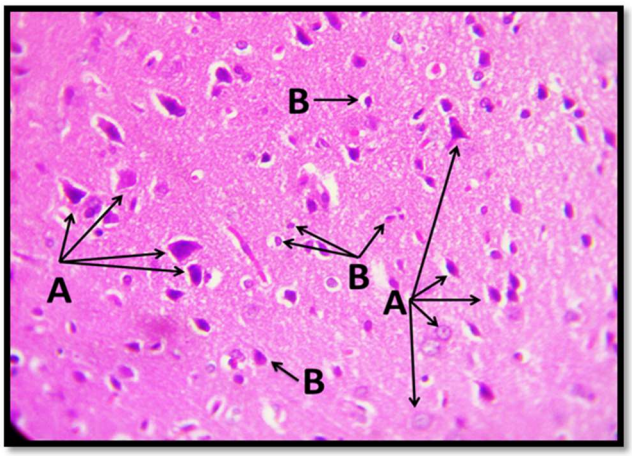

Figure (3-20): A microscopic image of a section in the brain of a mouse from the sixth group, in which the almost normal appearance of neurons with various shapes and sizes (A) is noted, in addition to glial cells (B), except for a slight vacuolation around them. (H&E, X40).(

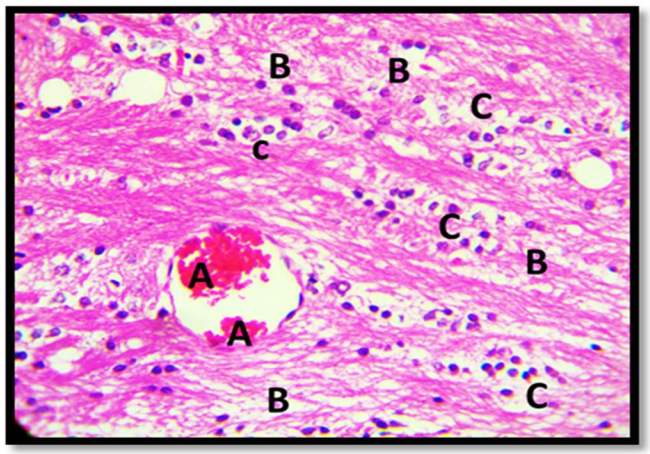

Figure (3-19): A microscopic image of a section of the brain of a mouse from the fifth group, in which thrombosis is observed in a dilated blood vessel (A), extensive vacuolation in nerve fibers (B), and glial cells in the form of clusters (C). (H&E, X40).

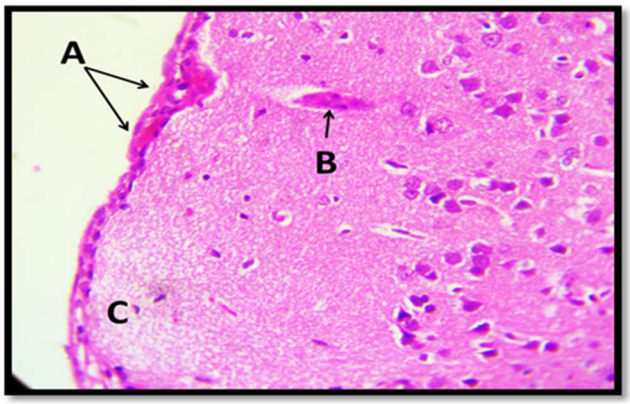

Figure (3-21): A microscopic image of a section in the brain of a mouse from the sixth group, in which blood congestion is observed at the periphery of the pia mater meningeal membrane (A) and in the molecular layer (B) with the disintegration of nerve fibers on one side (C). (H&E, X40).

Our results agree with Jeong *et al*. (2018) in a study of mice infected with *E. coli* O157:H7 which experienced neurological signs. Hemorrhage is observed in the lining of the blood vessels of the brain and spinal cord, as well as the edema. The current results also agree with a study by Mohawk *et al*. (2010) in the appearance of necrotic lesions in the brain, and reduction in Purkinje cells in the cerebellum. In a study conducted by Saito *et al.* (2019), they observed lesions of neurons in the cerebral cortex and myelin sheath, with edema in the cerebral cortex and spinal cord causing acute encephalopathy. In the same year, a study was conducted on dogs experimentally infected with *E. coli* O157:H7 and the results of histological examination of the cerebral cortex and cerebellum showed the presence of acute neuronal necrosis and slight reduction in Purkinje cells. These changes were attributed to excessive poisoning with Stx2 toxin (Li *et al.*, 2019). In a study in 2016 it is shown that the lesions in the brain are due to the presence of Gb3/CD77 receptors on the endothelial cells of the brain, as the toxin binds with these receptors and then enters the cells and inhibits protein synthesis, thus leading to cell death (Hasan, 2016).

The explanation for the occurrence of tissue lesions in the brain is due to the ability of Stx toxin to reach it and cross the blood-brain barrier. This barrier consists of tight junctions called tight ties around the capillaries that work effectively to prevent pathogens from entering the brain. The weakness of this barrier as a result of infection with E. coli O157:H7 is due to the presence of important proteins called TJ on its surface that bacteria destroy, which leads to its disruption or damage, and thus the invasion of bacteria and toxins into brain tissue (Li *et al*., 2019). In another explanation, it is attributed to the Tumor Necrosis Factor (TNF-α), which activates neutrophils and lymphocytes, and increases the permeability of vascular endothelial cells during the inflammatory process. The infection with *E. coli* O157:H7 significantly increases TNF expression -α in brain tissue. Moreover, meningitis is associated with increased TNF-α in brain tissue (Cheng *et al*., 2018). The cause of brain tissue lesions following *E. coli* O157:H7 infection can be attributed to hypoxia due to vasculopathy.

References

- **Ali, S. A. (2012).** A study of the effect of Zamzam water and the antibiotic Azithromycin on the morphological changes and histological lesions caused by *Escherichia coli* in some organs of albino mice. Msc Thesis/ College of Science- University of Tikrit.
- **Al-Taie, K. M. AR. (2020).** Isolation and pathogenicity study of virulent *Escherichia coli* in dogs. Msc Thesis/ College of Veterinary Medicine - University of Tikrit.
- **Cheng, Y.; Desse, S.; Martinez, A.; Worthen, R. J.; Jope, R. S. and Beurel, E. (2018).** TNFα disrupts blood brain barrier integrity to maintain prolonged depressive-like behavior in mice. *Brain Behav. immun.,* (69): 556-567.
- **Dulo, F. (2014).** Prevalence and antimicrobial resistance profile of *Escherichia coli* O157:H7 in goat slaughtered in dire dawa municipal abattoir as well as food safety knowledge , attitude and hygiene practice assessment among slaughter staff, Ethiopia. MSc, Thesis, Addis Ababa University.
- **Fatima, R. and Aziz, M. (2019).** Enterohemorrhagic *Escherichia coli* (EHEC). StatPearls; StatPearls Publishing: Treasure Island, FL, USA.
- **Feng, P.; Weagant, S. D. and Jinneman, K. (2014).** Prevalence and diversity of enterotoxigenic *Escherichia coli* strains in fresh produce. *J. Food Prot.,* 77(5): 820-823.
- **Hasan, M. S.; Yousif, A. A. and Alwan, M. J. (2016).** Detection of virulent genes in *E. coli* O157:H7 isolated from puppies and adult dogs by polymerase chain reaction. *Res. J. Vet. Pract*., 4(1): 1-6.
- **Jeong, Y. J.; Park, S. K.; Yoon, S. J.; Park, Y. J. and Lee, M. S. (2018).** Experimental in vivo models of bacterial Shiga toxin-associated hemolytic uremic syndrome. *J. Microbiol. Biotechnol*., 28(9): 1413-1425.
- **Klaif, S. F.; Saleh, Z. F.; Hussein, M. T.; Jawad, A. A. and Jawad, M. S. (2019).** Molecular characterization of enterohemorrhagic *E. coli* O157 and O153 isolated from tissue camel and human stool samples in Al-Diwaniyah, Iraq. *Iraqi J. Vet. Sci.*, 33(1): 81-86.
- **Legros, N.; Pohlentz, G., Steil, D. and Müthing, J. (2018).** Shiga toxin-glycosphingolipid interaction: Status quo of research with focus on primary human brain and kidney endothelial cells. *Int. J. Med. Microbiol.*, 308(8): 1073-1084.
- **Li, X.; Zhang, Z.; Chang, X.; Wang, X.; Hu, J.; Lin, Q. and Wang, X. (2019).** Disruption of blood-brain barrier by an *Escherichia coli* isolated from canine septicemia and meningoencephalitis. *Comp. Microbiol. Infect. Dis.,* (63): 44-50.
- **Luna, L. (1968).** Manual of histological staining methods of the Armed Forces Institute of Pathology. 3rd ed., The Blakiston Division. McGraw- Hill Book Co. New York. U.S.A.
- **Mahdi, E. M. (2019).** Histological comparison of the effect of the antibiotic ciprofloxacin and the aqueous and alcoholic extracts of Petroselinum crispu (Mineral) on a number of internal organs of albino mice experimentally infected with *E.coli*. Msc Thesis/ College of Science- University of Tikrit.

- **Mohawk, K.; Melton-Celsa, A.; Zangari, T.; Carroll, E. and O'Brien, A. (2010).** Pathogenesis of *Escherichia coli* O157:H7 strain 86-24 following oral infection of BALB/c mice with an intact commensal flora. *Microb. Pathog*., 48(3-4): 131-142.
- **Nair, A. B. and Jacob, S. (2016).** Asimple practice guide for dose conversion between animals and human. *J. Basic Clin. Pharm*., (7): 27-31.
- **Nguyen, T.; Le Van, P.; Huy Le, C. H . and Weintraub, A. (2005).** Antibiotic Resistance in Diarrheagenic *Escherichia. Vietnam Antimicrob. Agents Chemother.,* 49(2): 816-819.
- **Obrig, T. G. (2010).** *Escherichia coli* Shiga toxin mechanisms of action in renal disease. *Toxins*, 2(12): 2769-2794.
- **Reed, L. J. and Muench, H. (1938).** A simple method of estimating fifty percent end point. *A. J. Hyg.,* 27(3): 493-497
- **Saito, K.; Suzuki, R.; Koyanagi, Y.; Isogai, H.; Yoneyama, H. and Isogai, E. (2019).** Inhibition of enterohemorrhagic *Escherichia coli* O157: H7 infection in a genobiotic mouse model with pre-colonization by Bacteroides strains. *Biomed Rep.,* 10(3): 175-182.
- **Sejal, M. and Leonard, R. K. (2015).** *Escherichia coli* Infections. *Ped. Rev.,* 36(4): 4-176.
- **Tawfiq, J. A. (2006).** Increasing antibiotic resistance among isolates of *Escherichia coli* recovered from inpatients and outpatients in a Saudi Arabian hospital. *Infect. Control Hosp. Epidemiol.,* 27(7): 748-753.
- **Tse, C.; Yin, J.; Donowitz, M.; Doucet, M.; Foulke-Abel, J. and Kovbasnjuk, O. (2018).** Enterohemorrhagic *E. coli* (EHEC) Secreted Serine Protease EspP Stimulates Electrogenic Ion Transport in Human Colonoid Monolayers. *Toxins,* 10(9): 351.
- **Yadav, M.; Bhatiani, A.; Bhagoliwal, A.; Kumar, A. and Sujatha, R. (2018).** *Esherichia coli* O157: H7 Serotypes Isolation from Children in Stool Samples. *J. Pure. Appl. Microbiol.,* 12(1): 55-58.